



Prediction of crack location and propagation in stretch flanging process of aluminum alloy AA-5052 sheet using FEM simulation

Y. DEWANG¹, M. S. HORA², S. K. PANTHI³

1. Department of Mechanical Engineering, Maulana Azad National Institute of Technology, Bhopal 462051, India;
2. Department of Civil Engineering, Maulana Azad National Institute of Technology, Bhopal 462051, India;
3. Council of Scientific and Industrial Research, Advanced Materials and Processes Research Institute, Bhopal 462064, India

Received 22 August 2014; accepted 18 March 2015

Abstract: The stretch flanging process is significantly affected by various geometrical, material and process parameters. The punch-die clearance and initial flange length are main parameters which have major effects on the edge crack location and strain distribution along die profile radius in the flange. Non-axisymmetric stretch flanging process of AA-5052 sheet metal blanks was carried out by numerical simulation to predict the deformation behavior of flange, location and propagation of crack in flange and to investigate the effect of punch die clearance, flange length, die and punch profile radius and friction in the stretch flanging process. The experimental investigations were made to validate the simulations results. The results reveal that the crack length increases with the increase in the flange length. It is found that the flange length has a significant effect in circumferential direction as compared with the radial direction. The punch die clearance has the most significant effect in crack propagation in comparison with flange length. The circumferential strain is found to be larger in the case of punch having the profile radius less than the die profile radius, which leads to faster edge crack propagation. A close agreement is found between simulation and experimental results in terms of location of edge crack and forming load.

Key words: stretch flanging process; finite element simulation; punch-die clearance; initial flange length; edge crack

1 Introduction

The flanging is one of the most important sheet metal forming processes, which is generally used in automobile industries and many fabrication industries. It is used to make the smooth rounded edge, higher rigidity or strength at the edge of sheet-metal parts. The flanging is classified as shrink and stretch flanging on the basis of deformation behavior involved in the process. In shrink flanging process, the curvature of flange is convex and metal remains in compression along the circumferential direction. The arc length of final flange is smaller than that of the original element. In the stretch flanging process, the curvature of flange is opposite to shrink flanging, i.e., the curvature of flange is concave and sheet metal undergoes tension in circumferential direction. The feasibility of any sheet metal forming process depends upon various geometric, material and process parameters. In order to obtain defect-free

products, these parameters need to be optimized. This makes the process successful without causing failure in the form of necking, wrinkling and fracture. In recent years, it has become easier to predict such type of defects with finite element simulation at low cost and time, which is involved in the experimental investigations.

Many researchers, in the past, have made lots of investigations in the area of failure analysis in different sheet metal forming processes using finite element simulation. BRUNET et al [1] predicted necking in square cup deep drawing process using the modified Gurson's model. TEIXEIRA [2] coupled the Hill's orthotropic plasticity criterion with Lemaitre's ductile damage model and implemented it in the ABAQUS/Explicit code for the prediction of fracture in sheet metal forming process. LI et al [3] applied the Mohr–Coulomb fracture criterion in deep drawing process of AHSS using circular and square punch for prediction of shear induced fracture in terms of crack initiation, propagation and location of cracks. WU et al [4] predicted the failure in

deep drawing of nickel sheet using continuum damage mechanics approach. NGUYEN et al [5] used forming limit diagram ductile fracture criteria in deep drawing of steel plate cold rolled commercial grade (SPCC) material for prediction of wrinkles and fracture by FE simulation. KACEM et al [6] predicted necking, damage, fracture and limit in hole flanging process using a macroscopic ductile fracture criterion. WANG et al [7] investigated wrinkling effect in the shrink flanging process by using energy approach based on the stress-based criterion. HU et al [8] proposed an analytical model for introflexion/stretch and outcurve/shrink flange process considering the effect of planar anisotropy. DUDRA and SHAH [9] used stretch flanging model to a closed form solution for the axisymmetric case and FEM for non-axisymmetric case to find the trim line and peak strain. BAO and HUH [10] proposed a one-step analysis method to find out the feasible trimming line to obtain a precise final part shape after flanging. An equivalent 2D FEM was developed by WANG et al [11] to study the effect of various materials and process parameters in the stretch flanging of V-shaped blanks. LI et al [12] made further investigations in the stretch flanging process of V-shaped metal blanks and carried out elastic-plastic large deformation FEM. YEH et al [13] found optimum blank shape by using forward-inverse prediction scheme in the stretch flanging process, which integrates explicit dynamic FEM, true strain method and adaptive-network-based fuzzy inference system. WANG et al [14] developed an approximate theory and failure criteria for shrink and stretch flanging process and implemented it in a computer program. ASNAFI [15] made analytical and experimental investigations to study vertical stretch and shrink flanging of sheet. WORSWICK and FINN [16] carried out explicit dynamic finite element simulation of stretch flange forming operations utilizing various quadratic and non-quadratic yield criteria. FENG et al [17] studied the stretch flanging process and recommended small flange height and small ratio of straight side length to the curved range radius to avoid fracture at edge of flange. A multi-scale finite element damage percolation model was employed by CHEN et al [18] to simulate stretch flange forming of AA-5182 and AA-5754. A lower bound damage-based model was proposed by BUTCHER et al [19] for prediction of radial and circumferential cracks in stretch z-flanges of AA-5182. The continuum mechanics-based approach was developed by SIMHA et al [20] for prediction of radial and circumferential cracks in AA-5182 stretch flanges on the basis of extended stress-based forming limit curve.

In the present work, the finite element simulation of non-axisymmetric stretch flanging of AA-5052 sheet metal blanks was carried out using ABAQUS/Explicit

software. The effects of geometric parameters such as punch-die clearance, initial flange length, punch & die profile radius and friction were presented in terms of circumferential strain, radial strain and crack location in the flange. The crack initiation in the flange and its propagation with respect to punch displacement were studied extensively in terms of damage distribution. A number of experiments are performed to validate the simulation results.

2 Mechanical properties of material

The mechanical properties of aluminum alloy Al-5052 sheet were evaluated as per standard methods of tension testing method E8/E8M–11 ASTM by DAVIS et al [21]. The tensile specimens were tested on a computerized UTM (INSTRON) at a strain rate of 0.16667 s^{-1} along the rolling direction at room temperature. The true stress–strain curve obtained from tensile test is shown in Fig. 1. The chemical composition and mechanical properties of AA-5052 are provided in Tables 1 and 2, respectively.

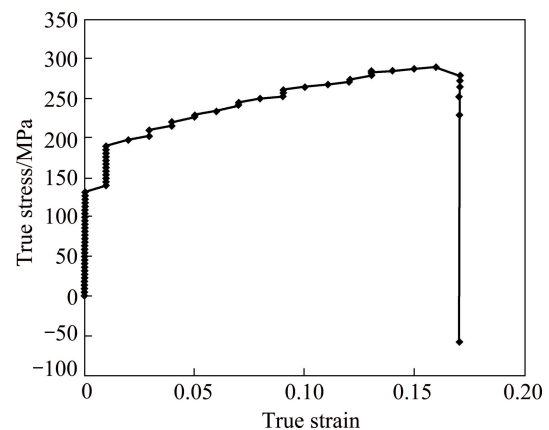


Fig. 1 True stress–strain curve for AA-5052

Table 1 Chemical composition of AA-5052 (mass fraction, %)

Si	Fe	Mg	Mn	Cu
0.122	0.196	.418	0.077	0.0362
Cr	Ni	Zn	Al	
0.167	0.004	0.044	95.700	

Table 2 Mechanical properties of AA-5052

Mass density/ ($\text{kg}\cdot\text{m}^{-3}$)	Elastic modulus/ GPa	Poisson ratio
2680	70.3	0.33

3 Finite element simulation

The finite element simulation of stretch flanging process was performed using commercially available

software ABAQUS/Explicit [22]. AYARI et al [23] used similar approach using ABAQUS for FEM simulation of square cup drawing process. The finite element discretization of components of stretch flanging set up is shown in Fig. 2.

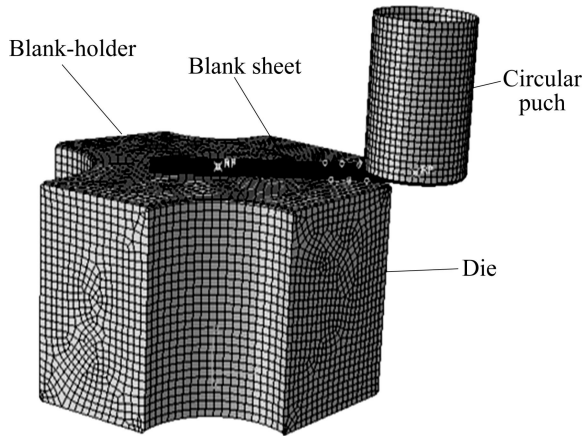


Fig. 2 Finite element discretization of non-axi-symmetric components of stretch flanging set up

The rectangular sheet metal blank (120 mm×25 mm) having thickness of 0.5 mm was considered in the present study. A gap of 0.1 mm was provided between the blank-holder and the top surface of the sheet to avoid initial penetration during contact. The punch, die and blank-holder were considered as a rigid body and the sheet was considered as a deformable body in the simulation process. The rigid bodies were modeled as rigid surfaces in the simulation using 4-node bilinear quadrilateral discrete rigid 3D (R3D4) elements having three translational degrees of freedom. The punch was modeled with 1738 elements and 1765 nodes. The blank-holder was modeled with 5883 elements and 5958 nodes and the die with 1283 elements and 1356 nodes. The rectangular sheet was modeled with 3D (C3D8R) 8500 elements and 17442 nodes in a single layer. The number of elements and nodes was varied for each case. The ductile and shear damage criteria were considered for isotropic hardening in the finite element simulation. The failure of flange was predicted by defining the

damage initiation criterion as a function of equivalent plastic strain. The damage evolution feature with element deletion technique was defined to predict the initiation and propagation of crack in the flange. The crack initiation took place when ductile damage parameter (D) became unity. The complete process of simulation was carried out in a number of small incremental steps. A mass of 1.1 N and a load of 20 kN at reference nodes were applied to blank-holder. The blank-holder was allowed to move in vertical direction to accommodate changes in blank thickness. The coefficient of friction was considered as 0.1 between contact surfaces. The die was fixed in all directions and the sheet was considered as a free body which was controlled by the contact boundary condition. The movement of punch was defined using a pilot node to obtain the punch force. The punch was allowed to move vertically downwards and restrained in all other directions. The evaluated mechanical properties of material were used in the FEM simulation. Figure 3 shows the variation of stress during formation of flange in various stages of punch displacement (u).

4 Experimental

In order to validate the results of finite element simulation, experimental results of stretch flanging process are obtained using hydraulic press equipped with a load cell of 2 kN. The experimental tool set up used in the present study is shown in Fig. 4. The tool setup comprises of punch, die and blank-holder with a rectangular sheet metal blank. The experiments were carried out by clamping the work piece between blank-holder and die by using four bolts of M10 size. A constant blank-holder force of 20 kN was applied during the tests by tightening the bolts with mechanical torque wrench. A constant rate of displacement 10 mm/min was applied to punching for formation of flange over the die. The punch displacements and punch load were continuously recorded in a data acquisition system. The experimental results are obtained considering similar geometrical and process conditions as that for simulation

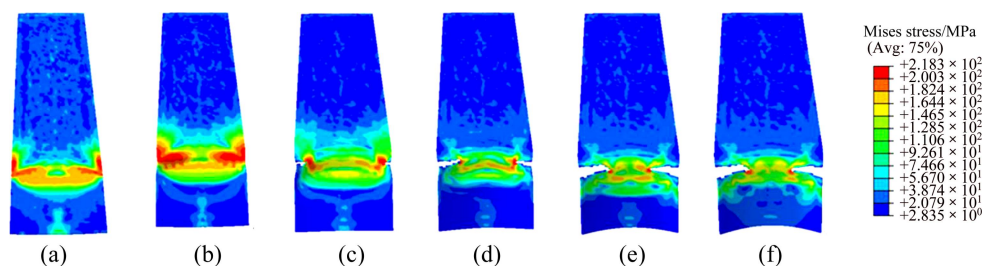


Fig. 3 Stress contour generated in flange at different punch displacements: (a) $u=1$ mm; (b) $u=3$ mm; (c) $u=5$ mm; (d) $u=6$ mm; (e) $u=10$ mm; (f) $u=20$ mm

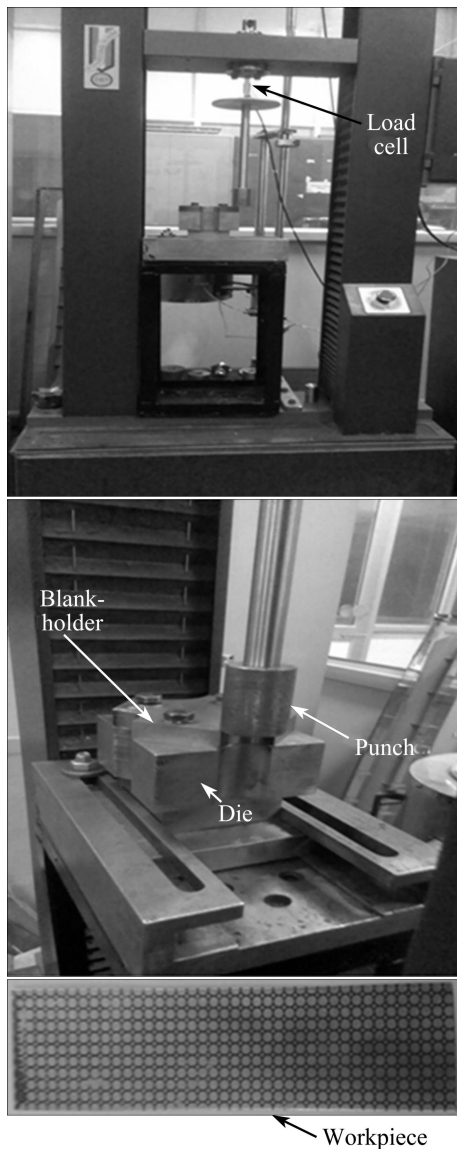


Fig. 4 Experimental tool and workpiece

for validation. The FEM simulation results are compared with the experimental results in terms of load–displacement curve and location of crack in the flange.

5 Results and discussion

5.1 Validation of simulation results

The results of simulation are validated with experimental results in terms of edge crack location, and load of forming in terms of load–displacement curves.

5.1.1 Comparison of edge crack location

To validate the predicted crack location by finite element simulation, the experiments were conducted at different punch die clearances of 1.0, 1.5, 2.0, 2.5 and 3.0 mm. The comparisons of edge crack location by simulation and experimental study at different punch-die clearances (c) at flange length of 30 mm are shown in Figs. 5 and 6. It is found that crack initiates from both ends and propagates toward center of the sheet along die profile radius in all cases. The length of propagation of crack decreases with increase in punch-die clearance. The maximum crack length is observed at $c=1.0$ mm while the minimum crack is observed at $c=3.0$ mm by simulation as well as experiment. The simulation results suggest that the smaller the punch-die clearance, the higher the circumferential strain which leads to edge cracking along the die profile radius.

Figures 7 and 8 show the comparison of FEM simulation and experimental results in terms of edge crack location and its propagation in the flange. These are presented with flange lengths (L) of 20, 30 and 40 mm at punch-die clearance of 1 mm to find out the effect of flange length on crack. It is found that the crack originates from both ends along die profile radius in all cases. The crack length increases with the increase in

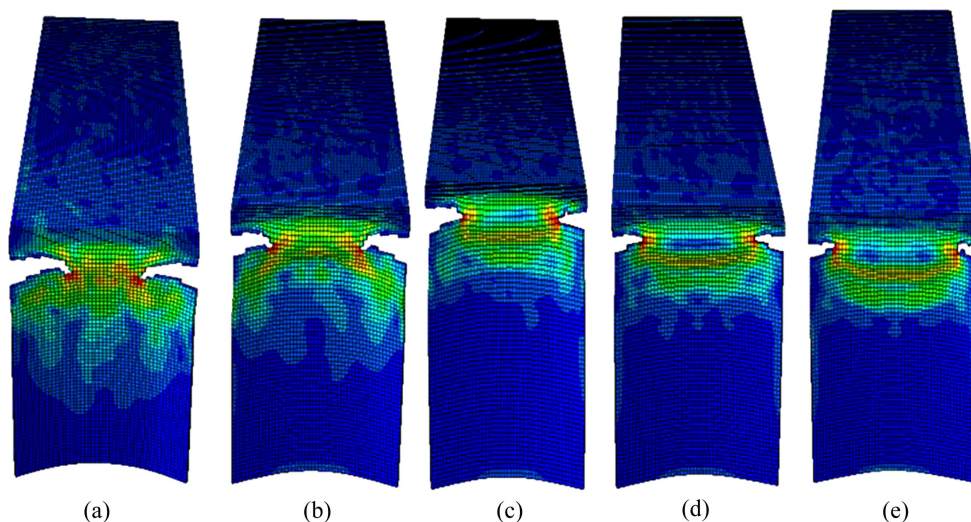


Fig. 5 Edge crack location in flange at different punch-die clearances by simulation: (a) $c=1.0$ mm; (b) $c=1.5$ mm; (c) $c=2.0$ mm; (d) $c=2.5$ mm; (e) $c=3.0$ mm

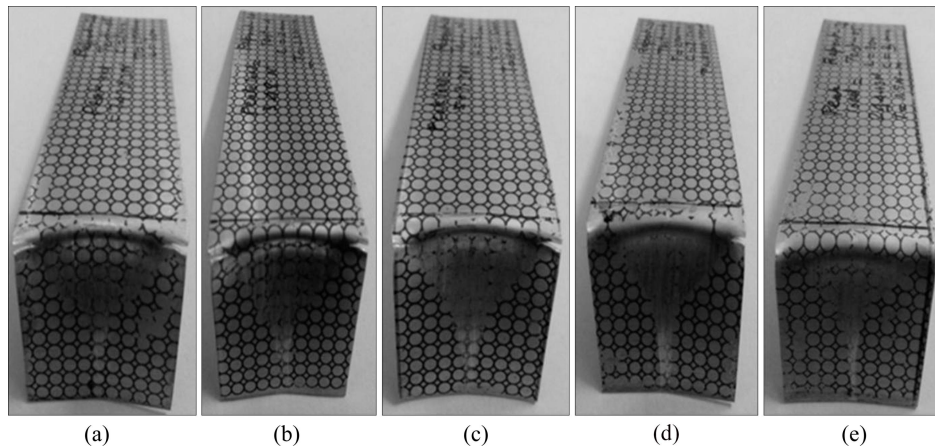


Fig. 6 Edge crack location in flange at different punch-die clearances by experiment: (a) $c=1.0$ mm; (b) $c=1.5$ mm; (c) $c=2.0$ mm; (d) $c=2.5$ mm; (e) $c=3.0$ mm

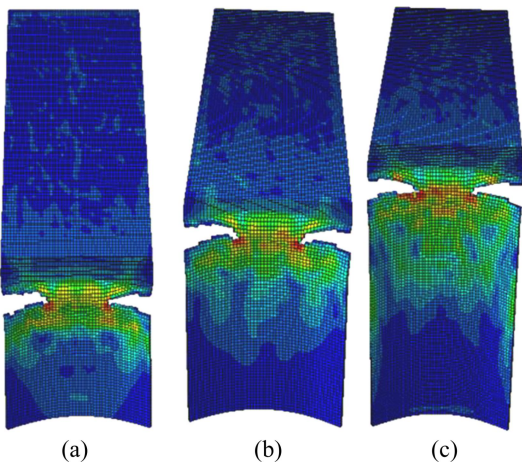


Fig. 7 Edge crack location in flange with different initial flange lengths by simulation: (a) $L=20$ mm; (b) $L=30$ mm; (c) $L=40$ mm

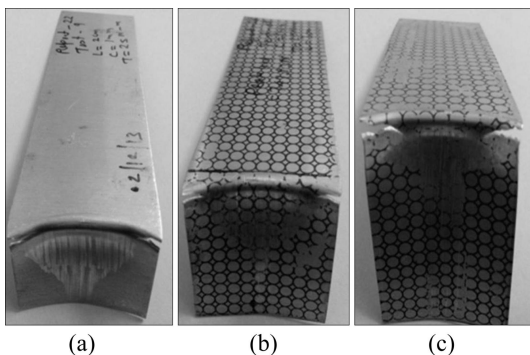


Fig. 8 Edge crack location in flange with different initial flange lengths by experiment: (a) $L=20$ mm; (b) $L=30$ mm; (c) $L=40$ mm

initial flange length because of increase in circumferential strain, which, in turn, leads to edge crack along die profile radius. A good agreement is found between simulation and experimental results in terms of crack length in flange.

5.1.2 Comparison of punch load

Figures 9–11 show plots of punch load vs punch displacement with flange lengths of 20, 30 and 40 mm respectively considering punch-die clearance of 1 mm. It is found that punch load increases with the increase in punch displacement (until the sheet does not incline by a certain amount). The maximum increase in punch load is found between 5 and 8 mm of punch displacement, which signifies that initial unbent or un-deformed portion of sheet requires higher load to bend the sheet along die profile radius. Further, the displacements of punch cause decrease in the punch load which is due to the sliding of punch over sheet or initiation of crack in sheet at the die corner. After the punch displacement of nearly 10 mm, punch load decreases gradually due to complete propagation of crack or sliding of punch over the flange. The same behavior is observed for all flange lengths. The simulation and experimental results suggest that higher punch load is required to form the flange in case of higher flange length. Figures 9–11 show a close agreement between simulation and experimental results.

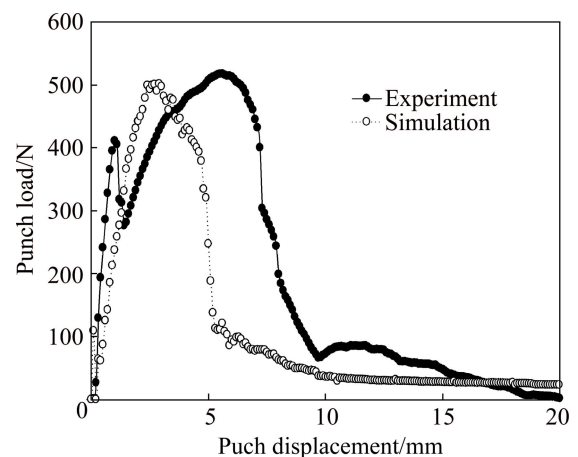


Fig. 9 Punch load–displacement curves for initial flange length of 20 mm

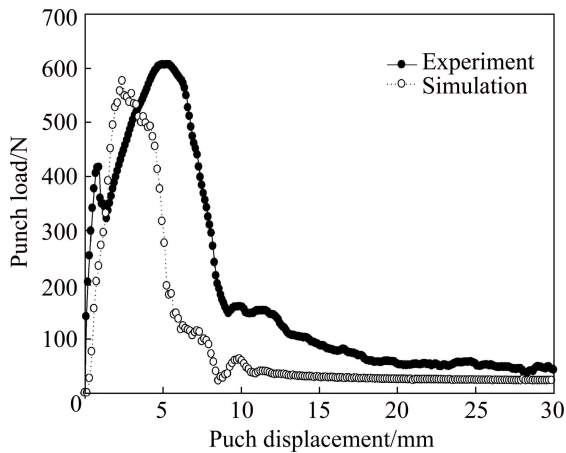


Fig. 10 Punch load–displacement curves for initial flange length of 30 mm

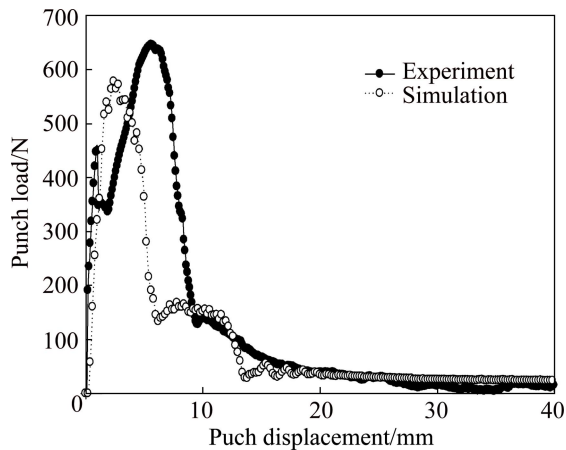


Fig. 11 Punch load–displacement curves for initial flange length of 40 mm

Figures 12 and 13 show the deformation behaviour of sheet at punch displacements of 5, 10, 15 and 20 mm with flange length of 20 mm. The crack initiation takes place in the sheet at the punch displacement of 5 mm by FEM simulation when the ductile damage parameter becomes unity while it starts, nearly, at punch displacement of 6 mm in the case of experimental study. As the punch moves vertically downwards, the sheet

deforms and forms the flange by following the die profile. The crack initiation and its propagation in the flange are depicted in Figs. 12 and 13. The predicted deformation behavior of sheet is found similarly in simulation and experiment.

5.2 FEM simulation results

5.2.1 Effect of punch-die clearance

The clearance between punch and die is one of the most important parameters in the stretch flanging process, which significantly influences the deformation behavior of the sheet. The effect of punch-die clearance is presented in terms of circumferential and radial strain distribution in flange. The strain distribution is predicted at die profile radius by defining a meridian path in the deformed sheet. A meridian path is shown in Fig. 14(a)

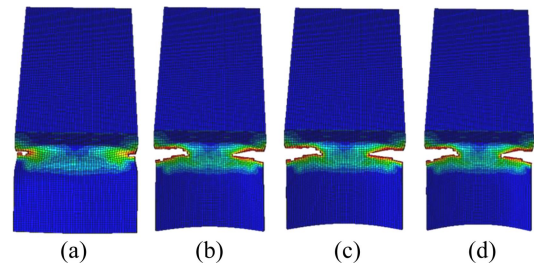


Fig. 12 Comparison of punch stroke between stretch flanging by simulation with initial length of 20 mm: (a) $u=5$ mm; (b) $u=10$ mm; (c) $u=15$ mm; (d) $u=20$ mm

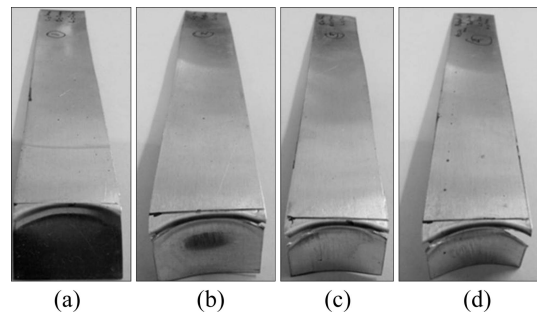


Fig. 13 Comparison of punch stroke between stretch flanging by experiment with initial length of 20 mm: (a) $u=5$ mm; (b) $u=10$ mm; (c) $u=15$ mm; (d) $u=20$ mm

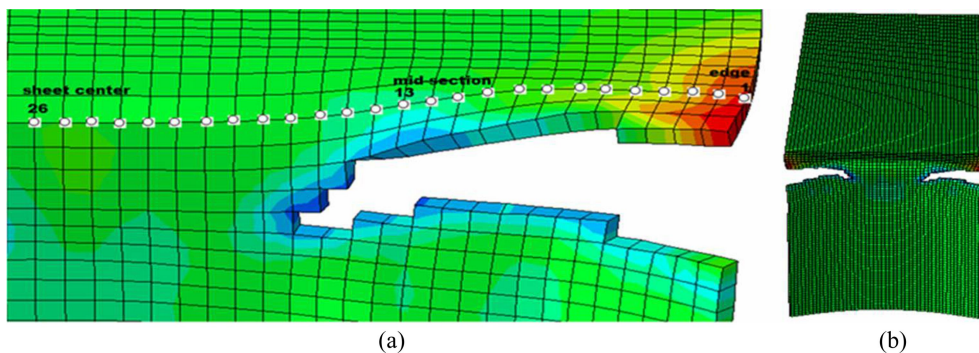


Fig. 14 Path for determination of circumferential strain near crack for flange length of 30 mm

with flange length of 30 mm and punch-die clearance of 1.0 mm. The path profile consists of total 26 nodes on right-half portion of the flange starting from the 1st node at edge to the 26th node at center of the sheet.

In the similar manner, meridian paths are defined for different cases of punch-die clearance. It is found that circumferential strain reduces along the die profile radius from edge (1st node) to mid-section (13th node) of sheet and then increases up to sheet center (26th node). The maximum and minimum circumferential strains occur at edge (1st node) and at a mid-section (13th node) of the sheet, respectively. A plot of circumferential strain vs distance along profile radius from edge is shown in Fig. 15 with punch-die clearance varying from 1.0 to 3.0 mm. It is noteworthy that circumferential strain decreases with the increase in punch-die clearance by nearly 14% at corner edge (1st node).

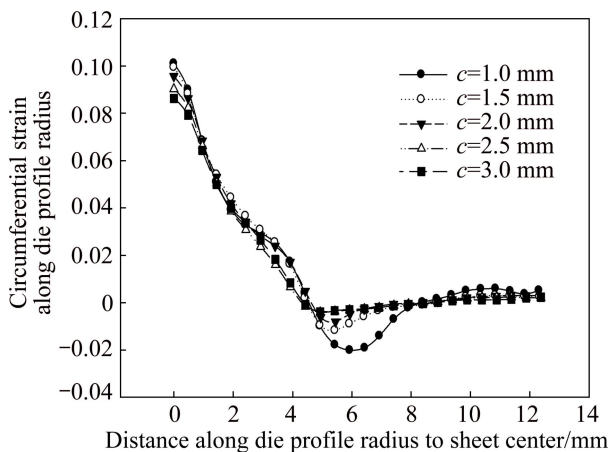


Fig. 15 Effect of punch-die clearance on circumferential strain

The effect of punch-die clearance on radial strain was studied and its contour plot is shown in Fig. 16. The plot between radial strain along die profile radius at different punch-die clearances (1.0 to 3.0 mm) is shown in Fig. 17. It is found that radial strain increases along die profile radius from edge (1st node) to a position near to mid-section of sheet (11th node) and thereafter, it

decreases up to the centre of the sheet (26th node). The maximum radial strain occurs at a position near to mid-section (11th node) of sheet and the minimum at edge (1st node) for all cases. The radial strain increases at corner edge by nearly 23% with increase in punch-die clearance from 1.0 mm to 3.0 mm.

5.2.2 Effect of initial flange length

The initial flange length is another important parameter which significantly affects the formability of stretch flange. In order to study the effect of flange length, a meridian path for one of the cases is arbitrarily chosen along die profile radius. A plot between radial strain and true distance along die profile radius up to the sheet center is shown in Fig. 18. It is found that the maximum radial strain occurs at a position near to mid-section (9th node) of the sheet while the minimum radial strain is found at the edge (1st node) of the flange along die profile radius. The insignificant increase of nearly 1% is found in the radial strain at the edges with increase in the flange length from 20 to 40 mm.

The same procedure is adopted to determine the circumferential strain along die profile radius. Figure 19 shows the variation of circumferential strain with the flange length. The meridian path method is considered as shown in Fig. 14. It is found that the maximum circumferential strain occurs at the edge (node 1) and the minimum at a position near to mid-position (node 14) of sheet for flange length of 40 mm. The circumferential strain increases nearly by 19% at edge (node 1) with increase in initial flange length from 20 to 40 mm. The variation in circumferential strain across the sheet is very large as compared with radial strain.

5.2.3 Effect of punch profile radius

Punch profile radius is another parameter that affects the edge crack location and its propagation. To find the effect of punch radius, FE simulation is performed for punch radii of 1, 2 and 3 mm. The effect of punch profile radius is presented in terms of variation in circumferential strain along die profile radius, which is shown in Fig. 20. The maximum circumferential strain in

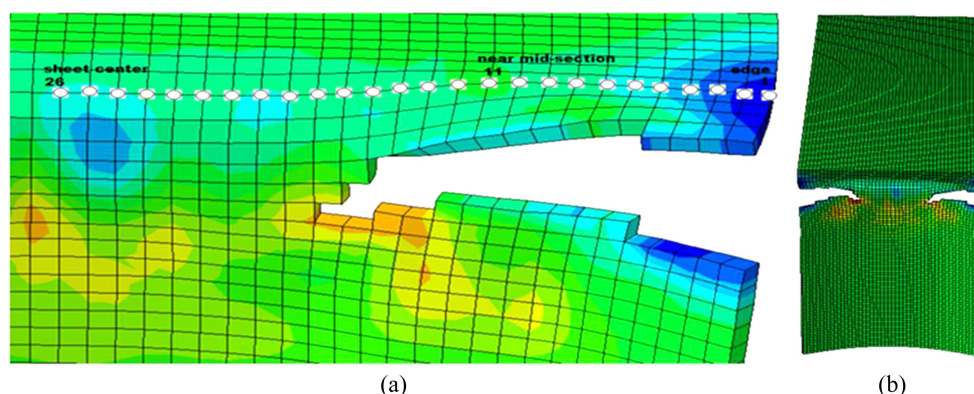


Fig. 16 Path for determination of radial strain near crack for flange length of 30 mm

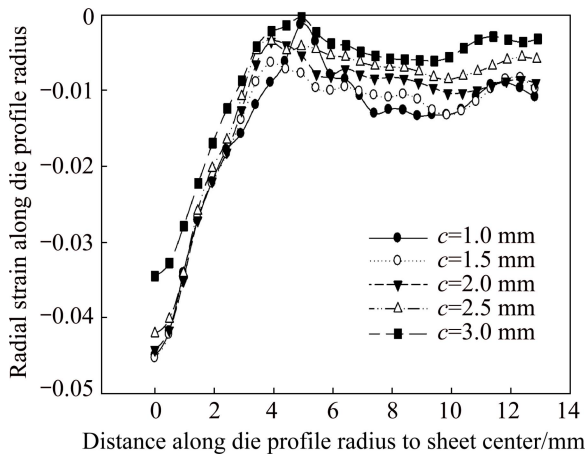


Fig. 17 Effect of punch-die clearance on radial strain

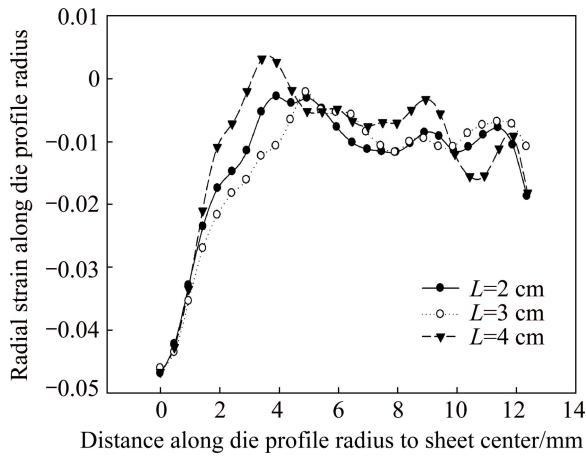


Fig. 18 Effect of initial flange length on radial strain

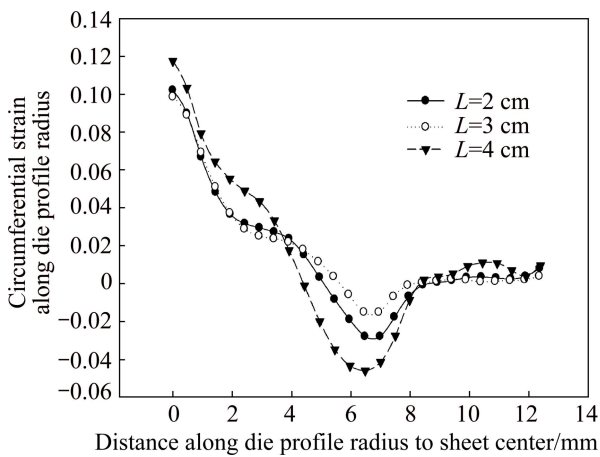


Fig. 19 Effect of initial flange length on circumferential strain

the flange with respect to punch profile radius is shown in Fig. 21. A similar procedure is adopted for obtaining circumferential strain distribution by observing a meridian path along the die profile radius. It is found from Fig. 20 that the maximum circumferential strain occurs at the edge of the sheet whereas it has negligible change towards center of the sheet. It is found that circumferential strain decreases with increase in the

punch profile radius at edge of the sheet. The maximum circumferential strain is obtained for the minimum punch profile radius while the minimum circumferential strain is obtained for the maximum punch profile radius. Figure 21 shows that the circumferential strain slightly decreases with increase in punch profile radius (R_p) from 1 to 3 mm. The punch profile radius has a less effect on crack location and its propagation. Figure 22 shows the effect of punch profile radius on crack location and propagation. It is found that crack initiates and propagates from the edge of sheet to center of sheet. The maximum crack propagation occurs for the minimum punch profile radius whereas the minimum propagation occurs for the maximum punch profile radius.

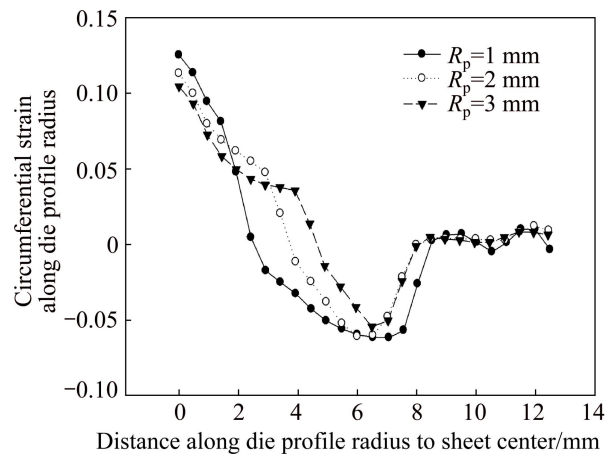


Fig. 20 Effect of punch profile radius on circumferential strain distribution along die profile radius

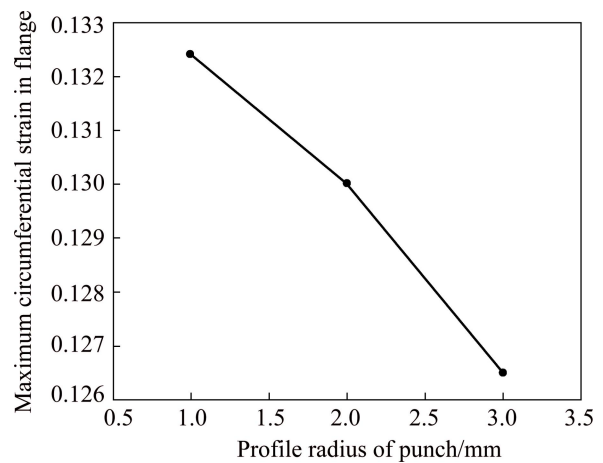


Fig. 21 Effect of punch profile radius on maximum circumferential strain

5.2.4 Effect of die profile radius

Die profile radius (R_d) is another geometric parameter that affects the edge crack location and its propagation. The effect of die profile radius was carried out considering die radii of 1, 2 and 3 mm and its effect is presented in terms of circumferential strain along die profile radius and the maximum circumferential strain in

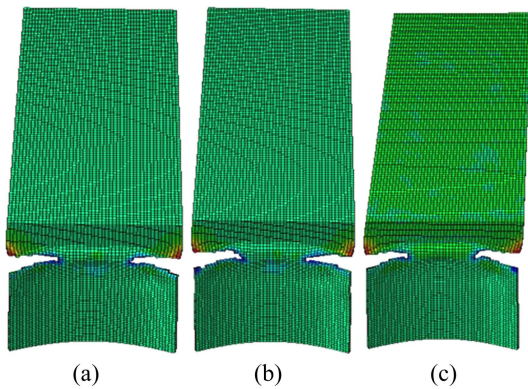


Fig. 22 Effect of punch profile radius on edge crack location and propagation: (a) $R_d=1$ mm, $R_p=1$ mm; (b) $R_d=1$ mm, $R_p=2$ mm; (c) $R_d=1$ mm, $R_p=3$ mm

flange. Figure 23 shows the variation of circumferential strain along the die profile radius for different die radii. It is found that the maximum circumferential strain occurs at the edge of the sheet whereas the minimum circumferential strain occurs at center of the sheet. The maximum circumferential strain decreases nearly by 9% with decrease in die profile radius from 1 to 3 mm, as shown in Fig. 24. The maximum edge crack propagation occurs in the case of the maximum die profile radius as depicted from Fig. 25. The results reveal that the circumferential strain is higher in the case of punch having the profile radius less than die profile radius, which leads to greater edge crack propagation. Therefore, a punch having larger profile radius than die profile radius should be used to minimize the length of crack in the flange.

5.2.5 Effect of coefficient of friction

The coefficient of friction (μ) between contacting surfaces such as die, punch, blank-holder and blank is the most important parameters, which influences the circumferential strain as well as edge crack location and propagation. In order to establish the effect of coefficient

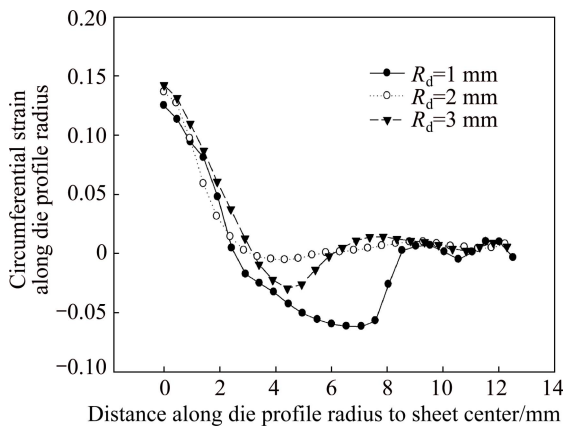


Fig. 23 Effect of die profile radius on circumferential strain distribution along die profile radius

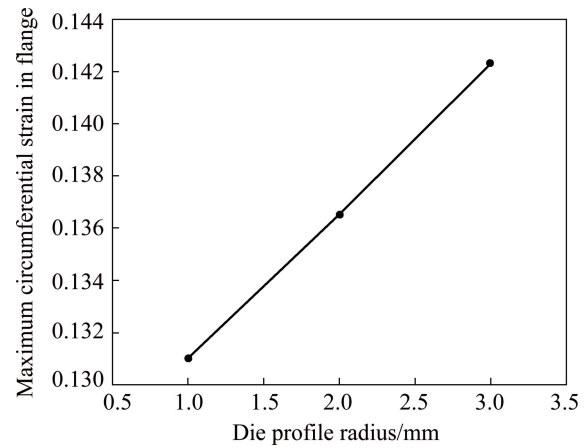


Fig. 24 Effect of die profile radius on maximum circumferential strain in flange

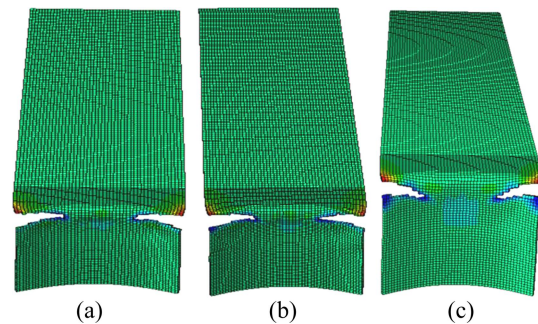


Fig. 25 Effect of die profile radius on edge crack location and propagation: (a) $R_d=1$ mm, $R_p=1$ mm; (b) $R_d=2$ mm, $R_p=1$ mm; (c) $R_d=3$ mm, $R_p=1$ mm

of friction, a constant blank-holding force of 500 N is considered for all three cases. Figure 26 shows the effect of coefficient of friction on circumferential strain distribution along die profile radius. The results are presented in terms of circumferential strain distribution and the maximum strain in the flange. Figures 26 and 27 show that the maximum circumferential strain increases with the increase in coefficient of friction, which results in higher crack propagation. It is found that the maximum circumferential strain occurs at edge of sheet, whereas, the minimum is found at the center of the sheet. Figure 28 shows the effect of coefficient of friction on edge crack location and propagation

5.2.6 Failure distribution

Figure 29 shows the damage distribution in terms of ductile damage and shear damage criterion at various punch displacements. It is found that damage increases with the increase in punch displacement along a die profile radius. The minimum failure is found at the sheet center while the maximum at edge of the sheet corresponding to each punch displacement. It is found that, when the punch displacement is 4 mm, the damage is less than unity and it becomes 1.0, at edge of the sheet,

at punch displacement of nearly 5 mm. This shows the initiation of crack in the flange. The damage parameter remains unity at edge of the sheet for further displacement of punch, but it increases towards the centre of sheet results in propagation of crack towards the center of the flange.

The contours for ductile and shear failure initiation

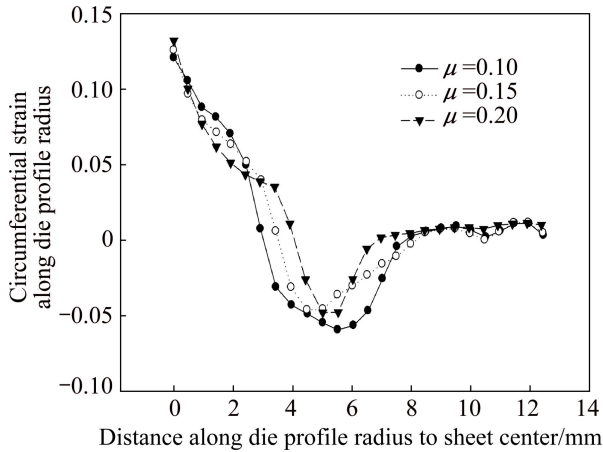


Fig. 26 Effect of coefficient of friction on circumferential strain distribution along die profile radius

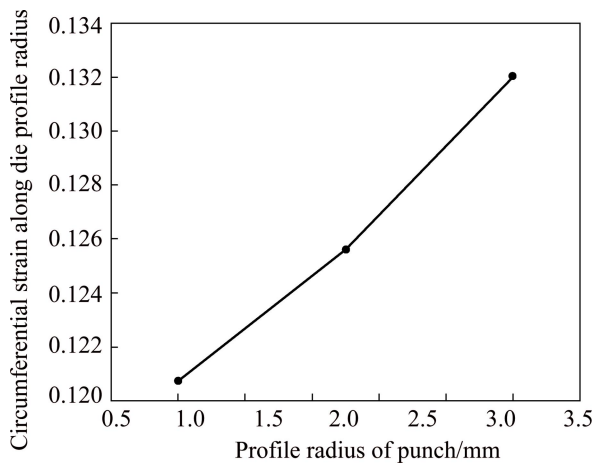


Fig. 27 Effect of coefficient of friction on maximum circumferential strain in flange

criteria are depicted in Figs. 30 and 31 respectively at punch displacements of 5, 10, 15 and 20 mm.

Figure 32 shows the damage distribution considering ductile damage criterion and shear damage criterion at the center of flange, which is initially free from the crack for various punch displacements. It is found that spread of damage increases with increase in the punch displacement along a path near to die profile

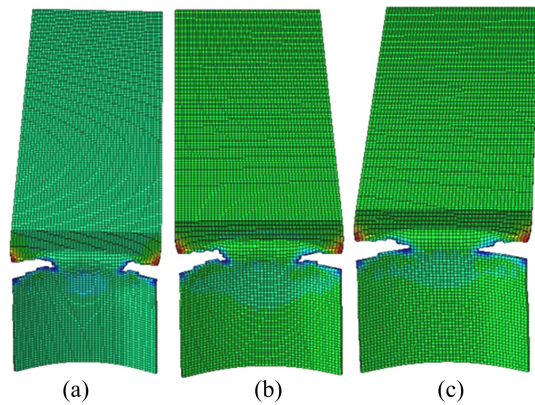


Fig. 28 Effect of coefficient of friction on edge crack location and propagation: (a) $\mu = 0.10$; (b) $\mu = 0.15$; (c) $\mu = 0.20$

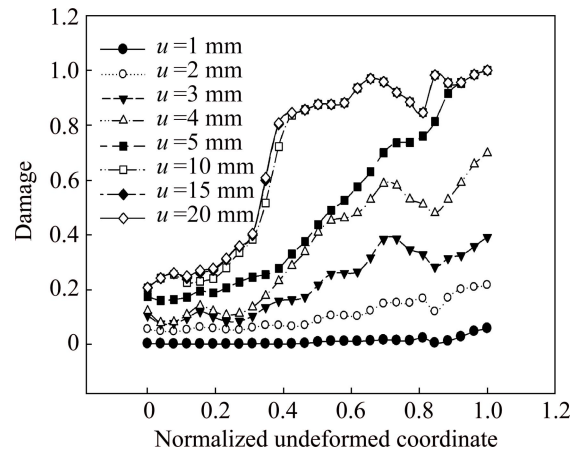


Fig. 29 Damage distribution along die profile radius from center to edge

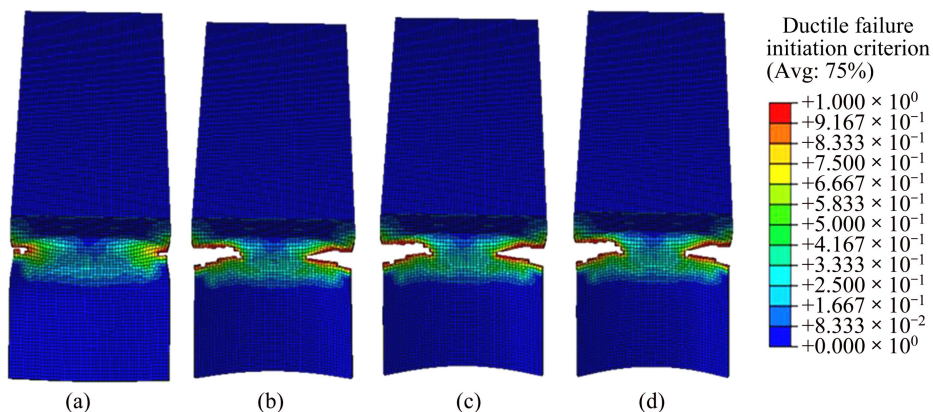


Fig. 30 Ductile failure initiation criterion distribution by simulation at punch displacements of 5 mm (a), 10 mm (b), 15 mm (c) and 20 mm (d)

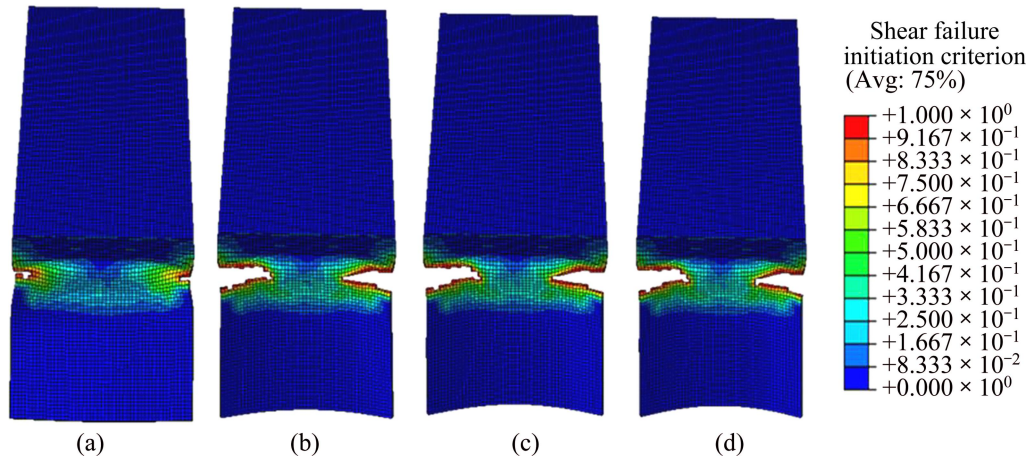


Fig. 31 Shear failure initiation criterion distribution by simulation at punch displacements of 5 mm (a), 10 mm (b), 15 mm (c) and 20 mm (d)

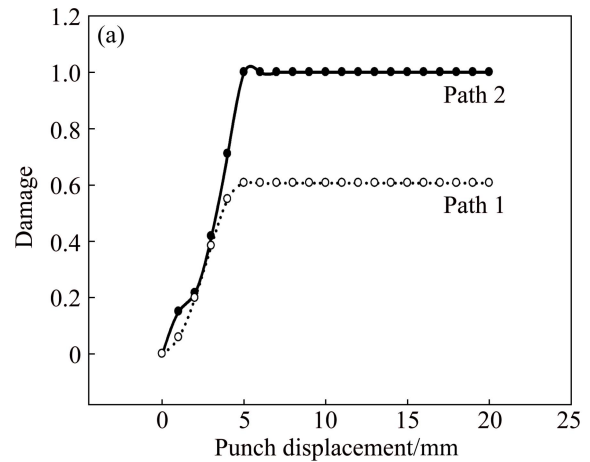
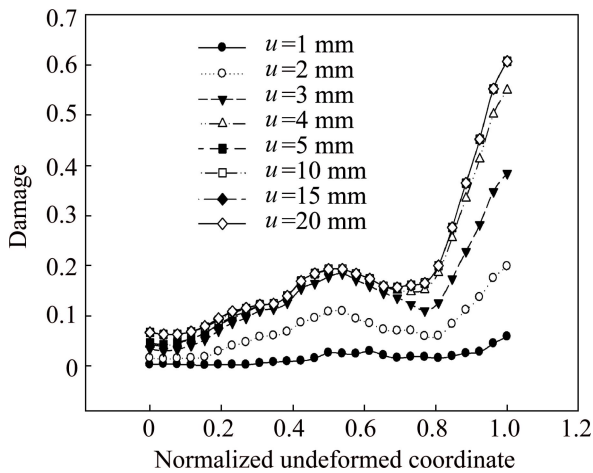


Fig. 32 Damage distribution along path near to die profile radius from center to edge

radius. Thus, the crack initiation and propagation can be predicted using the ductile and shear damage criterion. It shows a crack free zone where damage parameter is less than unity.

Figure 33 (a) shows relationship between damage (based on ductile damage criterion and shear failure criterion) and punch displacement. The damage distribution is plotted for two different paths, i.e., Path 1 and Path 2, as shown in Fig. 33(b). Path 1 is selected in a crack free zone while Path 2 is selected near to the crack zone. The maximum damage obtained at each increment of punch displacement is depicted in Fig. 33(a). It is found that for Path 2, damage increases with the increase in punch displacement initially and it reaches 1.0 at punch displacement of 5 mm, causing crack initiation in flange. At further displacement of punch, the damage remains unity at edges and it increases towards the centre of sheet (up to unity), which indicates the crack propagation in the flange. In the similar manner,

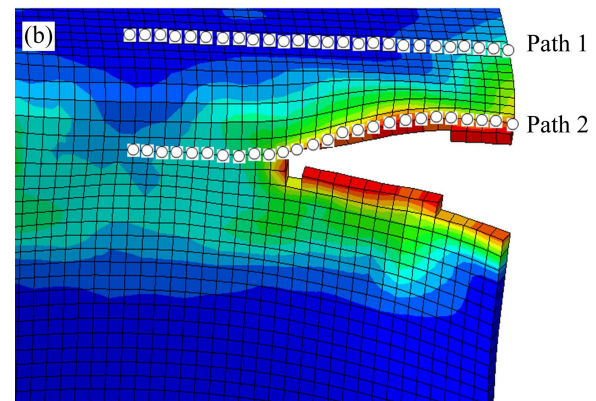


Fig. 33 Relationship between damage and punch displacement for different regions along die profile radius (a) and magnified path along safe zone and along fractured zone of stretch flange (b)

damage distribution is plotted for Path 1. The damage increases with the increase in punch displacement from 1 to 5 mm and it attains the maximum value of 0.607, thereafter, it remains constant for further displacement of punch which shows a crack free zone in the flange.

6 Conclusions

1) The crack length increases with increase in initial flange length due to increase in circumferential strain which leads to edge crack along die profile radius.

2) The circumferential strain decreases nearly by 14% and radial strain increases approximately by 23% at edge with the increase in punch-die clearance from 1 to 3 mm. Thus, the punch-die clearance has significant effects on the crack propagation in the flange.

3) The 19% increase in circumferential strain is found at the edge when initial flange length increases from 20 to 40 mm, whereas, a insignificant change (nearly 1%) is found in the radial strain. Thus, the flange length has a significant effect on circumferential strain as compared with radial strain.

4) Higher forming load is required to form the stretch flange in the case of higher flange length.

5) The circumferential strain decreases approximately by 5% and increases nearly by 9% with the increase in punch and die profile radii respectively at the flange edge.

6) Punch-die profile radii have significant effects in a combined manner on circumferential strain and edge crack propagation. Therefore, a punch having larger profile radius than die should be used preferably.

7) Circumferential strain increases by 10% nearly with the increase in coefficient of friction. The greater the coefficient of friction, the greater the edge cracking will be and it propagates towards sheet center. Thus, coefficient of friction also plays a significant role in distribution of circumferential strain and edge crack and propagation.

Acknowledgements

The authors would like to thank the Science and Engineering Research Board (SERB), Department of Science & Technology, Government of India for financially supporting this research.

References

- [1] BRUNET M, SABOURIN F, TOUCHAL M S. The prediction of necking and failure in 3D: Sheet forming analysis using damage variable [J]. *Journal De Physique*, 1996, 6: 473–482.
- [2] TEIXEIRA P. Finite element prediction of ductile fracture in sheet metal forming processes [J]. *Journal of Materials Processing Technology*, 2006, 177: 278–281.
- [3] LI Y, LUO M, GERLACH J, WIERZBIC T. Prediction of shear-induced fracture in sheet metal forming [J]. *Journal of Materials Processing Technology*, 2010, 210: 1858–1869.
- [4] WU J, MA Z, ZHOU Y, LU C. Prediction of failure modes during deep drawing of metal sheets with nickel coating [J]. *Journal of Materials Science & Technology*, 2013, 29: 1059–1066.
- [5] NGUYEN D T, DINH D K, NGUYEN H M, KIM Y S. Formability improvement and blank shape definition for deep drawing of cylindrical cup with complex curve profile from SPCC sheets using FEM [J]. *Journal of Central South University*, 2014, 21: 27–34.
- [6] KACEM A, KRICHEN A, MANACH P Y, THUILLIER S, YOON J W. Failure prediction in the hole-flanging process of aluminum alloys [J]. *Engineering Fracture Mechanics*, 2013, 99: 251–265.
- [7] WANG X, CAO J, LI M. Wrinkling analysis in shrink flanging [J]. *Journal of Manufacturing Science and Engineering*, 2001, 123: 426–432.
- [8] HU P, LI D Y, LI Y X. Analytical models of stretch and shrink flanging [J]. *International Journal of Machine Tools & Manufacture*, 2003, 43: 1367–1373.
- [9] DUDRA S, SHAH S. Stretch flanges: Formability and trimline development [J]. *Journal of Materials Shaping Technology*, 1998, 6: 91–101.
- [10] BAO Y D, HUH H. Optimum design of trimming line by one-step analysis for auto body parts [J]. *Journal of Materials Processing Technology*, 2007, 187–188: 108–112.
- [11] WANG N M, JOHNSON L K, TANG S C. Stretch flanging of “V”-shaped sheet metal blanks [J]. *Journal of Applied Metalworking*, 1984, 3: 281–291.
- [12] LI D, LUO Y, PENG Y, HU P. The numerical and analytical study on stretch flanging of V-shaped sheet metal [J]. *Journal of Materials Processing Technology*, 2007, 189: 262–267.
- [13] YEH F H, WU M T, LI C L. Accurate optimization of blank design in stretch flange based on a forward-inverse prediction scheme [J]. *International Journal of Machine Tools & Manufacture*, 2007, 47: 1854–1863.
- [14] WANG C T, KINZEL G, ALTAN T. Failure and wrinkling criteria and mathematical modeling of shrink and stretch flanging operations in sheet-metal forming [J]. *Journal Materials Processing Technology*, 1995, 53: 759–780.
- [15] ASNAFI N. On stretch and shrink flanging of sheet aluminium by fluid forming [J]. *Journal of Materials Processing Technology*, 1999, 96: 198–214.
- [16] WORSWICK M J, FINN M J. The numerical simulation of stretch flange forming [J]. *International Journal of Plasticity*, 2000, 16: 701–720.
- [17] XU Feng, LIN Zhong-qin, LI Shu-hui, XU Wei-li. Study on the influences of geometrical parameters on the formability of stretch curved flanging by numerical simulation [J]. *Journal of Materials Processing Technology*, 2004, 145(1): 93–98.
- [18] CHEN Z, WORSWICK M J, PILKEY A K, LLOYD D J. Damage percolation during stretch flange forming of aluminum alloy sheet [J]. *Journal of the Mechanics and Physics of Solids*, 2005, 53: 2692–2717.
- [19] BUTCHER C, CHEN Z, WORSWICK W. A lower bound damage-based finite element simulation of stretch flange forming of Al-Mg alloys [J]. *International Journal of Fracture*, 2006, 142: 289–298.
- [20] SIMHA C M, GRANTAB R, WORSWICK M J. Application of an extended stress-based forming limit curve to predict necking in stretch flange forming [J]. *Journal of Manufacturing Science and Engineering*, 2008, 130: 1–11.
- [21] DAVIS J R, DAVIS A. *Tensile testing* [M]. 2nd ed. Ohio: ASM International, 2004.
- [22] ABAQUS/EXPLICIT. *User manual* [M]. Version 6.10. Providence Rhode Island: Dassault Systemes Simulia Corporation, 2011.
- [23] AYARI F, LAZGHAB T, BAYRAKTAR E. Parametric finite element analysis of square cup deep drawing [J]. *Archives of Computational Materials Science and Surface Engineering*, 2009, 1: 106–111.

5052 铝板拉伸翻边工艺中的裂纹位置和扩展预测的有限元模拟

Y. DEWANG¹, M. S. HORA², S. K. PANTHI³

1. Department of Mechanical Engineering, Maulana Azad National Institute of Technology, Bhopal 462051, India;

2. Department of Civil Engineering, Maulana Azad National Institute of Technology, Bhopal 462051, India;

3. Council of Scientific and Industrial Research, Advanced Materials and Processes Research Institute,
Bhopal 462064, India

摘 要: 拉伸翻边工艺受多种几何形状、材料和工艺参数的影响。冲模间隙和初始翻边长度是影响边界裂纹位置和沿模侧面半径应力分布的主要参数。采用数值模拟研究 AA-5052 铝板的非轴对称拉伸翻边工艺, 预测翻边的变形行为、裂纹位置和扩展, 并且研究拉伸翻边过程中冲模间隙、翻边长度、冲模外形半径和摩擦力的影响。利用实验研究对模拟结果进行验证。结果表明, 裂纹长度随翻边长度的增加而增加, 翻边长度在周向的影响比在轴向的影响大, 冲模间隙比翻边长度对裂纹扩展的影响更大。当冲孔外形半径比模的外形半径小时, 周向应变增加, 这导致了较快的边裂纹扩展。在边裂纹位置和变形负载方面, 模拟结果和实验结果较好吻合。

关键词: 拉伸翻边工艺; 有限元模拟; 冲模间隙; 初始翻边长度; 边裂纹

(Edited by Xiang-qun LI)